UKAEA-CCFE-PR(19)37

K. Arakawa, M.-C. Marinica, S. Fitzgerald, L. Proville, D. Nguyen-Manh, S. L. Dudarev, P.-W. Ma, T. D. Swinburne, A. M. Goryaeva, T. Yamada, T. Amino, S. Arai, Y. Yamamoto, K. Higuchi, N. Tanaka, H. Yasuda, T. Yasuda, H. Mori

Observation of quantum de-trapping and transport of heavy defects in tungsten

Observation of quantum de-trapping and transport of heavy defects in tungsten

K. Arakawa, M.-C. Marinica, S. Fitzgerald, L. Proville, D. Nguyen-Manh, S. L. Dudarev, P.-W. Ma, T. D. Swinburne, A. M. Goryaeva, T. Yamada, T. Amino, S. Arai, Y. Yamamoto, K. Higuchi, N. Tanaka, H. Yasuda, T. Yasuda, H. Mori

This is a preprint of a paper submitted for publication in Nature Materials

Observation of quantum de-trapping and transport of heavy defects in tungsten

Kazuto Arakawa[1*], Mihai-Cosmin Marinica[2], Steven Fitzgerald[3], Laurent Proville[2], Duc Nguyen-Manh[4], Sergei L. Dudarev[4], Pui-Wai Ma[4], Thomas D. Swinburne[5], Alexandra M. Goryaeva[2], Tetsuya Yamada[6], Takafumi Amino[7], Shigeo Arai[8], Yuta Yamamoto[8], Kimitaka Higuchi[8], Nobuo Tanaka[8], Hidehiro Yasuda[9], Tetsuya Yasuda[9], Hirotaro Mori[9]

[1]*Next Generation TATARA Co-Creation Centre, Innovation Creation Organization, Shimane University, 1060 Nishikawatsu, Matsue 690-8504, Japan.*

[2]*DEN-Service de Recherches de Métallurgie Physique, CEA, Université Paris-Saclay, F-91191, Gif-sur-Yvette, France.*

[3]*Department of Applied Mathematics, University of Leeds, Leeds LS2 9JT, UK*

[4]*CCFE, United Kingdom Atomic Energy Authority, Culham Science Centre, Oxfordshire OX14 3DB, United Kingdom.*

[5]*CINaM-Aix Marseille Université-CNRS, 13009 Marseille, France.*

[6]*Railway, Automotive & Machinery Parts Unit Osaka Steel Works, Nippon Steel & Sumitomo Metal Corporation, 1-109, Shimaya 5-chome, Konohana-ku, Osaka 554-0024, Japan.*

[7]*Advanced Technology Research Laboratories, Nippon Steel & Sumitomo Metal Corporation, 1-8 Fuso-Cho, Amagasaki, Hyogo 660-0891, Japan.*

[8]*Institute of Materials and Systems for Sustainability, Nagoya University, Nagoya 464-8603, Japan.*

[9]*Research Centre for Ultra-High Voltage Electron Microscopy, Osaka University, 7-1 Mihogaoka, Ibaraki, Osaka 567-0047, Japan.*

*email: arakawa@riko.shimane-u.ac.jp

The diffusion of defects in crystalline materials[1] governs macroscopic behaviour in a wide range of processes, including alloying, precipitation, phase transformation, and creep[2]. In real materials, intrinsic defects are unavoidably bound to static trapping centres such as impurity atoms, meaning that their diffusion is controlled by the de-trapping process. It is generally held that de-trapping occurs only by thermal activation. In this Letter we report the first direct observation of the quantum de-trapping of defects below around 1/3 of the Debye temperature. We successfully monitored the de-trapping and migration of self-interstitial atom clusters, strongly trapped by impurity atoms in tungsten, by triggering de-trapping out of equilibrium at cryogenic temperatures, using high-energy electron irradiation and in-situ transmission electron microscopy. The quantum-assisted de-trapping leads to low-temperature diffusion rates orders of magnitude higher than a naive classical estimate suggests. Our analysis shows that this phenomenon is generic to any crystalline material.

Under high-energy irradiation (or extreme mechanical deformation), atoms in a crystal can be displaced significantly from their lattice positions, forming vacancy and self-interstitial atom (SIA) defects. These are ultimately responsible for severe degradation in the mechanical properties of materials, such as hardening, swelling, and embrittlement[3]. Understanding the basic mechanisms controlling their formation and diffusion[4-6] is critical for the development of future next-generation energy systems.

In the field of material science, to the best of our knowledge, all observed migration processes of species heavier than H or He[7,8] have been interpreted as thermal activation characterized by the Arrhenius rate[9], or phonon dragging[10,11]; no apparent quantum effects have been detected[12], although they have been theoretically considered for SIAs[13-15] and screw dislocations[16]. Quantum effects have also been observed on metal surfaces[17]. We focus here on the low temperature diffusion of SIA clusters in tungsten as a model for crystal defects in heavy-atom systems.

The lowest-energy SIA configuration in tungsten (and the other non-magnetic body-centred-cubic (bcc) transition metals) is the ⟨111⟩ crowdion, in which atomic displacements are confined almost entirely to the ⟨111⟩ string containing the extra atom. The defect is delocalized: it involves many more than one atom, as the displacement field is spread down the string, resulting in very low barriers to translation (known as *Peierls* barriers, see Supplementary Discussion 1a and Fig. ED1). Hence crowdions perform one-dimensional (1D) diffusion along their axis with a low (meV scale) activation energy[10,18,19]. Similarly to single crowdions, SIA clusters in the form of **b** = ½⟨111⟩ dislocation loops undergo 1D glide diffusion in the direction of the Burgers' vector **b**. This phenomenon has been studied using classical molecular dynamics simulations (MD)[20-24] and transmission electron microscopy (TEM)[5,25] for α-iron and other metals and alloys.

According to MD studies, the activation energy (Peierls barrier) for cluster diffusion is less than 0.1 eV[20,22], meaning they are thermally mobile even at very low temperatures. In any real material however, impurity atoms (mainly carbon and nitrogen) act as traps by binding to the clusters. Vacancies (expected at high density under irradiation) will mutually annihilate with SIAs at the cluster boundary.

Previous studies, using resistivity recovery and internal friction experiments[9], have shown that low-temperature cluster migration in tungsten (and other bcc metals) is strongly influenced by the concentration of impurity atoms[26-28].

These traps are deep enough (~1 eV, see Supplementary Discussion 1b and Fig. ED2) to prevent TEM observation of the clusters' thermal escape and subsequent motion on experimental timescales, even at 300 K, and they remain immobile. To overcome this, we used the electron beam in transmission electron microscopes such as a high-voltage electron microscope (HVEM) to enhance the vacancy mobility and reduce the effective trap depth. In the absence of the electron beam, vacancies are immobile up to 620-900K[9], but in our experiment, the momentum imparted by the incident electrons moves the vacancies up to 100 times per second. The experimental system is shown schematically in Fig. 1, and operates as follows.

First, a high energy (2000 keV) electron beam is used to create displacement damage, vacancies and SIAs at 105 K, before aging at 300 K. This allows the SIA clusters to nucleate and grow to the nanoscale, bound to impurities at their perimeters (where the binding energy is greatest). At these temperatures, the vacancies are thermally immobile and remain dispersed throughout the sample. A lower energy (100-1000 keV) beam is then turned on the sample. These energies are too low to create additional vacancies and SIAs, but high enough to athermally move the existing vacancies (see Methods), and the previously trapped clusters begin to move (Fig. 1;

Supplementary Video 1). The principal quantity we monitor is the cluster motion frequency. The precise definition of this quantity, together with its dependence on the experimental irradiation conditions, is given in Methods and illustrated in Fig. 2. Perhaps the most striking feature of our study is its ability to resolve the SIA clusters' thermal and quantum-mechanical motion, even under a ballistic flux of vacancies. In Methods we describe in detail how this is possible.

The key features of the motion are:

i) hops are rare events, i.e. the clusters spend far more time trapped than travelling between traps;
ii) clusters sometimes move back and forth between fixed points in the sample;
iii) clusters are observed to shrink under the beam;
iv) motion frequency depends strongly on temperature.

i) and ii) tell us that the clusters are escaping from the impurity traps, moving quickly through the lattice before being subsequently trapped again; iii) tells us how: the radiation-mobilized vacancies move through the crystal, attracted to the high compressive strain at the cluster boundaries. Here they annihilate the SIAs at the cluster boundaries, shrinking the cluster, and increasing the separation between the impurity atom and the cluster boundary. The impurity-cluster interaction is strong but short-ranged (see Supplementary Discussion 1b and Fig. ED2), and falls off towards zero within a few lattice spacings, so the traps are now much shallower, and escape is easier (Fig. 2abc). We now turn to the temperature dependence, iv), which demonstrates that the low temperature escapes are quantum mechanical in nature.

Figure 3 is an Arrhenius plot showing the logarithm of the motion frequency vs. the inverse temperature. Hops due to thermal escape from potential wells of depth $\Delta V \gg k_{\mathrm{B}}T$ have a characteristic rate $\propto \exp(-\Delta V/k_{\mathrm{B}}T)$, i.e. a straight line on an

Arrhenius plot. This appears to be the case for the higher temperatures $T \geq 50$ K and the slope suggests ΔV is higher than 10 meV. As the temperature is reduced, 17 K $\leq T \leq$ 50 K, the slope flattens as the mechanism transitions from classical thermal escape towards temperature-independent quantum mechanical diffusion.

The measured rates result from three independent processes: the athermal radiation-driven vacancy migration under the beam (rate Γ_{vac}), the fluctuation-driven escape of the cluster from the trap (depth ΔV_{trap}, rate Γ_{trap}), and finally the traversal of the Peierls barrier intrinsic to the crystal (depth ΔV_{P}, rate Γ_{P}) (see Methods).

Figure 3a shows attempted classical fits for all barriers $10\mathrm{meV} \leq \Delta V = \Delta V_{\mathrm{P}} + \Delta V_{\mathrm{trap}} \leq 90\mathrm{meV}$. Note that the Peierls traversal rate is non-Arrhenius (since ΔV_{P} is not more than $k_{\mathrm{B}}T$, see Methods), but no possible classical form for the rate can explain the observed values. (We are confident that the sample temperatures continue to decrease below 50 K, and are not significantly increased by beam heating – see Supplementary Discussion 2 and Fig. ED3).

In Fig. 3b, we use a quantum mechanical form for the escape rate Γ^{QM}, derived from the quantized nature of the crystal phonons (see Methods). These obey Bose-Einstein rather than Boltzmann statistics, and their zero-point fluctuations increase the average energy available for the cluster to overcome the barrier, thus increasing the low temperature rates in excellent agreement with the experimental values. Moreover, the same quantum rates simultaneously fit two datasets acquired at different voltages. This proves that the same quantum mechanism underlies both datasets.

However, we still obtain acceptable fits for all barriers between 10 and 90 meV. To narrow this down, we considered the critical temperature τ_c below which classical physics breaks down (see Methods), which depends on the barrier height: Figure 2 shows the 90 meV fit clearly failing below 140 K, whereas the 10 meV one appears reasonable down to around 50 K. τ_c depends on the phonon density of states, and is estimated[29] to be 101 K for pure tungsten (about 1/3 of the Debye temperature). Fitted values for τ_c are also shown in Fig. 3, and the value 101 K is consistent with a barrier height of 30 – 44 meV. We note that the resistivity recovery and internal friction experiments obtain a barrier height of 15 – 60 meV[9,26-28].

Other manifestations of quantum behaviour are in principle possible, in particular the deep tunneling of the entire cluster. However, fitting the data to this functional form requires unrealistic values for the cluster's effective mass (see Methods), and we conclude that, over the range of temperatures probed by our experiment, quantized phonons facilitating the clusters' escape from traps 30 – 44 meV deep provide the optimal explanation of the data.

In this study we have performed the first direct investigation of cryogenic defect diffusion using in-situ TEM. Our unique experimental system allowed us to manipulate the effective potential wells encountered by SIA clusters, reducing their depth until we could probe the quantum mechanical nature of their de-trapping. The quantum transport becomes dominant below around 1/3 of the Debye temperature. Moreover, the behaviour derives from quantized phonons, which drive the stochastic fluctuations of objects that are themselves too heavy to tunnel significantly. This likely affects low temperature defect transport in many crystalline materials. Our results demonstrate the importance of quantum effects on low temperature defect evolution even in heavy atom systems.

References

1. Mehrer, H. *Diffusion in Solids*. Vol. 155 (Springer, 2007).
2. Gupta, D. *Diffusion Processes in Advanced Technological Materials*. (William Andrew Inc., 2005).
3. Gary, S. W. *Fundamentals of Radiation Materials Science*. (Springer, 2007).
4. Fu, C.-C., Torre, J. D., Willaime, F., Bocquet, J.-L. & Barbu, A. Multiscale modelling of defect kinetics in irradiated iron. *Nature Materials* **4**, 68-74 (2005).
5. Arakawa, K. *et al.* Observation of the one-dimensional diffusion of nanometer-sized dislocation loops. *Science* **318**, 956-959 (2007).
6. Bai, X.-M., Voter, A. F., Hoagland, R. G., Nastasi, M. & Uberuaga, B. P. Efficient Annealing of Radiation Damage Near Grain Boundaries via Interstitial Emission. *Science* **327**, 1631-1634 (2010).
7. Kadono, R. *et al.* Quantum diffusion of positive muons in copper. *Physical Review B* **39**, 23-41 (1989).
8. Sundell, P. G. & Wahnström, G. Activation energies for quantum diffusion of hydrogen in metals and on metal surfaces using delocalized nuclei within the density-functional theory. *Physical Review Letters* **92**, 155901 (2004).
9. Ehrhart, P., Jung, P., Schultz, H. & Ullmaier, H. *Atomic Defects in Metals*. Vol. 25 (Springer-Verlag, Berlin, 1991).
10. Derlet, P. M., Nguyen-Manh, D. & Dudarev, S. L. Multiscale modeling of crowdion and vacancy defects in body-centered-cubic transition metals. *Physical Review B* **76**, 054107 (2007).
11. Swinburne, T. D., Dudarev, S. L. & Sutton, A. P. Classical Mobility of Highly Mobile Crystal Defects. *Physical Review Letters* **113**, 215501 (2014).
12. Wollenberger, H. J. in *Physical Metallurgy, Part II* (eds R. W. Chan & P. Haasen) 1139 (North Holland Physics Publishing, Amsterdam, 1983).
13. Pushkarov, D. I. Quantum theory of crowdions at low temperatures. *Soviet Journal of Experimental and Theoretical Physics* **37** (1973).
14. Flynn, C. P. Resonance mode hopping and the stage I annealing of metals. *Thin Solid Films* **25**, 37-43 (1975).
15. Swinburne, T. D., Ma, P.-W. & Dudarev, S. L. Low temperature diffusivity of self-interstitial defects in tungsten. *New Journal of Physics* **19**, 073024 (2017).
16. Proville, L., Rodney, D. & Marinica, M.-C. Quantum effect on thermally activated glide of dislocations. *Nat Mater* **11**, 845-849 (2012).
17. Ohresser, P. *et al.* Surface Diffusion of Cr Adatoms on Au(111) by Quantum Tunneling. *Physical Review Letters* **95**, 195901 (2005).
18. Fitzgerald, S. P. & Nguyen-Manh, D. Peierls potential for crowdions in the bcc transition metals. *Physical Review Letters* **101**, 115504 (2008).
19. Amino, T., Arakawa, K. & Mori, H. Detection of one-dimensional migration of single self-interstitial atoms in tungsten using high-voltage electron microscopy. *Sci Rep* **6**, 26099 (2016).
20. Wirth, B. D., Odette, G. R., Maroudas, D. & Lucas, G. E. Dislocation loop structure, energy and mobility of self-interstitial atom clusters in bcc iron. *J Nucl Mater* **276**, 33-40 (2000).
21. Marian, J. *et al.* Dynamics of self-interstitial cluster migration in pure α-Fe and Fe-Cu alloys. *Physical Review B* **65**, 144102 (2002).

22 Osetsky, Y. N., Bacon, D. J., Serra, A., Singh, B. N. & Golubov, S. I. One-dimensional atomic transport by clusters of self-interstitial atoms in iron and copper. *Philos Mag* **83**, 61-91 (2003).

23 Dudarev, S. L. The non-Arrhenius migration of interstitial defects in bcc transition metals. *Comptes Rendus Physique* **9**, 409-417 (2008).

24 Swinburne, T. D., Dudarev, S. L., Fitzgerald, S. P., Gilbert, M. R. & Sutton, A. P. Theory and simulation of the diffusion of kinks on dislocations in bcc metals. *Physical Review B* **87**, 064108 (2013).

25 Arakawa, K., Amino, T. & Mori, H. One-dimensional glide motion of "naked" 1/2<111> prismatic dislocation loops in iron. *ISIJ International* **54**, 2421-2424 (2014).

26 Dausinger, F. & Schultz, H. Long-range migration of self-interstitial atoms in tungsten. *Physical Review Letters* **35**, 1773-1775 (1975).

27 Dausinger, V. F. Die Tieftemperaturerholung in elektronenbestrahltem Wolfram. *Philosophical Magazine A* **37**, 819-836 (1978).

28 Mizubayashi, H. & Okuda, S. Elastic after-effect studies of self-interstitials in tungsten after fast neutron irradiation at 5 K. *Radiation Effects* **54**, 201-215 (1981).

29 Ashcroft, N. W. & Mermin, N. D. *Solid State Physics*. (College Edition, New York, 1978).

Acknowledgements

This work was financially supported by JSPS KAKENHI (Grant No. 15H04244, and 18K18951), ImPACT Program of Council for Science, Technology and Innovation (Cabinet Office, Government of Japan), Q-LEAP Program (MEXT: Ministry of Education, Culture, Sports, Science and Technology - Japan), and the Iron and Steel Institute of Japan Research Promotion Grant. Part of this work was supported by the "Advanced Characterization Nanotechnology Platform, Nanotechnology Platform Programs" of MEXT, at Institute of Materials and Systems for Sustainability (Nanotechnology Open Facilities) in Nagoya University and at Research Centre for Ultra-High Voltage Electron Microscopy (Nanotechnology Open Facilities) in Osaka University, and TATARA Nanotechnology Project Centre in Shimane University. M.C.M. acknowledges support from the GENCI -(CINES/CCRT) computer centre under Grant No. A0050906973. A.M.G. and M.C.M acknowledges the financial support of the Cross-Disciplinary Program on Numerical Simulation of CEA, the French Alternative Energies and Atomic Energy Commission. S.P.F. acknowledges support from the UK EPSRC, grant number EP/R005974/1. The work at CCFE has been carried out within the framework of the EUROfusion Consortium and has received funding from the Euratom research and training programme 2019-2020 under grant agreement No 633053 and funding from the RCUK Energy Programme [grant number EP/P012450/1]. The views and opinions expressed herein do not necessarily reflect those of the European Commission.

Author contributions

K.A., M.C.M. and L.P. designed the study. K.A., T.Y., T.A., S.A., Y.Y., K.H., N.T., H.Y., T.Y. and H.M. performed the experiments. M.C.M., S.P.F., L.P., D.N.M., A.M.G., S.L.D., P.W.M. and T.D.S. performed the theoretical works. K.A., M.C.M., S.P.F., and S.L.D. wrote the main draft. All authors discussed the results and commented on the manuscript.

Additional information

Supplementary information is available in the online version of the paper. Reprints and permissions information is available online at www.nature.com/reprints. Correspondence and requests for materials should be addressed to K.A.

Competing financial interests

The authors declare no competing financial interest.

METHODS

Specimen preparation. We cut (011) discs from one grain of an ingot of high-purity coarse-grained polycrystalline tungsten (99.9999 mass % JX Nippon Mining & Metals Co., Tokyo, Japan; impurity amounts of the ingot are given in Ref. [30]). The discs were thinned to 0.1mm, using spark erosion and mechanical polishing, then perforated at the centre by electropolishing so the periphery of the hole became cross-sectionally wedge-shaped for TEM observations.

Production of SIA clusters. We used high-energy electron irradiation in a HVEM (Hitachi H-3000) to create SIAs and vacancies in the thin foil specimens. The acceleration voltage was 2000 kV, and a temperature of 105 K was maintained using a liquid-nitrogen-cooled specimen holder (Oxford Instruments). We note that the thermal migration of vacancies is frozen at temperatures below 620-900 K[9]. The beam flux was 1×10^{24} $m^{-2}s^{-1}$, and the dose was 4×10^{25} m^{-2}.

During 2000-keV electron irradiation, pairs of SIAs and vacancies are produced[31] via knock-on displacement. Based on our recent work[19,30], the point defect reactions proceed as follows: most of the highly mobile 1D-moving SIAs react with vacancies, or escape to the foil surface, where they are annihilated. Surviving SIAs bind to impurity atoms and form embryonic SIA clusters, that grow by absorbing other SIAs, and take the form of $\mathbf{b} = ½\langle 111 \rangle$ dislocation loops. These clusters are intrinsically highly mobile, yet they are trapped by impurities and remain stationary. Vacancies that do not react with SIAs accumulate throughout the irradiated area of the specimen.

Using TEM, the average size and density of the SIA formed clusters under the above condition were found to be approximately 3-4 nm and 4×10^{22} m^{-3}, respectively. Accumulated vacancies are not visible in the TEM. After the irradiation, the specimen was aged at approximately 300 K. This allows the clusters trapped by weak impurity atoms with shallow potential wells to thermally escape and move, leading to coalescence with other clusters[32], escape to the specimen surfaces, or to trapping by stronger impurities with deeper wells. However, even after aging for several months, we did not see any significant change in the cluster density, demonstrating that thermal escape of SIA clusters from the deeper wells hardly occurs even at 300 K.

TEM observation of the 1D motion of SIA clusters in response to high-energy

electron irradiation. We then used the electron beam to induce the vacancy mobility, with acceleration voltages of 100, 150, 300, 500 (Hitachi H-9000UHV), 1000, and 2000kV (H-3000) – all except 2000kV are below the threshold for point defect generation in tungsten[31]. Additional very intense irradiations were carried out at 1000kV using a JEOL JEM 1000K RS. Beam fluxes ranged from 5×10^{22} to 2×10^{25} $m^{-2}s^{-1}$, and temperatures ranged from 17-300 K (where no thermal migration of vacancies takes place[9]). We achieved these temperatures using liquid-helium-cooled specimen holders (Oxford Instruments), in which the temperature is measured with a thermocouple attached to the specimen mount, so the measured temperature is the average over the whole specimen.

The specimen thickness ranged from 50 to 70 nm (measured using equal-thickness fringes[33]). The observations were carried out using the weak-beam dark-field technique[34] with a reflection of **g** = 200. Under this condition, all SIA clusters in the form of prismatic dislocation loops with a **b** = ½⟨111⟩ type Burgers vector and a diameter greater than approximately 2 nm were imaged. The dynamic response of the clusters was monitored and recorded with CCDs having frame rates of 30 fps for H-9000UHV and H-3000, and 15 fps for JEM 1000K RS.

We define the motion frequency of the clusters as the ratio of the number of cluster hops observed per unit time divided by the number of observable clusters, i.e. the average motion frequency of individual SIA clusters.

Motion frequency and the ballistic and kinetic rates of SIA clusters. Our experiments measure the average motion frequency of SIA clusters as observed in the transmission electron microscopes. The average motion frequency is defined as $\nu_{\mathrm{MF}}(t) = n_{\mathrm{m}}/(n\,t)$: the ratio of the number of clusters that move (n_{m}) divided by the total number of observed clusters (n) in the observation time (t).

The measured rates ν_{MF} are the combined results of motion induced by directly by the irradiation, and stochastic motion induced by the underlying phonon bath. Consequently, the motion frequency is impacted by irradiation conditions, in particular the electron beam flux Φ and energy E. The temperature T also influences the experimental observations through the phonon bath, meaning that the motion frequency is a function defined on a 4 dimensional space $\nu_{\mathrm{MF}}(t, T, \Phi, E)$. Figure 3 illustrates the temperature dependence, and Fig. 2d-g shows the behaviour of the motion frequency with respect to the other variables. Here we derive an expression for the motion frequency in the context of the experiments.

Detailed experimental analysis suggests that the shrinkage of the clusters (Fig. 2a) originates from irradiation-induced vacancy motion (Fig. 2b). Since the impurities are immobile, the erosion of the clusters increases the distance between them and the impurities. We call the mechanism of the cluster de-trapping due to this process the *indirect de-trapping mechanism.* Since it depends on the radiation-mobilized vacancies eroding the SIA clusters, the cluster motion frequency is proportional to the vacancy concentration, c_{V}. These vacancies are absorbed by the clusters, and other sinks such as the specimen surface, at a rate proportional to the concentration itself: $\dot{c}_{\mathrm{V}} \propto -c_{\mathrm{V}}$. So long as no new Frenkel pairs are created, this leads to an exponential decay in time of the vacancy concentration, and hence the cluster motion frequency. This is precisely what we observe in Fig. 2cd, in the short time limit.

In the indirect mechanism, cluster de-trapping is also impacted by the thermal rate at which the clusters escape from the impurities. At a given cluster-impurity separation, d_k, sufficiently large that the trapping energy is low, the thermal escape rate Γ_{th}^{k} is governed by the cluster-impurity trapping energy $\Delta V_{\mathrm{trap}}^{k}$ for that distance (see next section). If we have n_k cluster-impurity sets at given cluster-impurity separation d_k, then the number of clusters that jump within the observation time is $a\, c_{\mathrm{V}} n_k\, \Gamma_{\mathrm{th}}^{k} t$. The factor a incorporates the impact of the beam flux and energy on the observations.

Since the incident electron energy is high, what we call the *direct de-trapping mechanism* – direct collision of the electron with the impurity that traps the cluster – can also release the cluster. The rate Γ_{d} of this direct mechanism is athermal and uniform in time, depending only on the concentration of cluster-trapping impurities and the flux and energy of the electrons. The probability to release a cluster from an impurity via the direct mechanism is $n\Gamma_{\mathrm{d}} t$.

Consequently, the measured motion frequency can be written as

$$\nu_{\mathrm{MF}} = \frac{n_{\mathrm{indirect}} + n_{\mathrm{direct}}}{n\, t} = \frac{\sum_k a c_{\mathrm{V}} n_k\, \Gamma_{\mathrm{th}}^{k}(T) t + n\Gamma_{\mathrm{d}} t}{nt}$$

Or, in a simpler form, if we assume that in the system the initial vacancy density $c_v(0)$ decreases in time with a decay factor α_v :

$$\nu_{\mathrm{MF}} \sim \sum_k a\, c_{\mathrm{V}}(0) e^{-\alpha_v t} \frac{\Gamma_{\mathrm{th}}^{k}(T) n_k}{n} + \Gamma_{\mathrm{d}} = e^{-\alpha_v t}\left[\sum_k a\, c_{\mathrm{V}}(0) \frac{\Gamma_{\mathrm{th}}^{k}(T) n_k}{n}\right] + \Gamma_{\mathrm{d}}$$

This theoretical expression for the motion frequency is fully compatible with all the experimental evidence described in the body of the paper and illustrated in Fig. 2.

Firstly, the experimental observations shown in Fig. 2de indicate that the motion frequency decreases exponentially in time, and after several hundred seconds, the frequency's exponential decay transitions to a constant plateau. This reflects the local exhaustion of vacancies near the clusters, and the transition to the direct mechanism. The $t \to \infty$ limit provides the frequency associated with the direct mechanism $\nu_{\mathrm{MF}} \to \Gamma_{\mathrm{d}}$. In the limit of $t \to 0$:

$$\nu_{\mathrm{MF}}(t \to 0) \to \left[\sum_k a_k c_v(0) \frac{\Gamma_{\mathrm{th}}^k(T) n_k}{n}\right] + \Gamma_{\mathrm{d}} \sim \text{const} \times \Gamma_{\mathrm{th}}^0(T) + \Gamma_{\mathrm{d}},$$

we have access, up to multiplicative (const) and additive (Γ_{d}) constants, to the dominant thermal/quantum rate $\Gamma_{\mathrm{th}}^0(T)$ on whose nature, classical or quantum, our study is focused. Moreover, the higher the beam energy, the greater the mobility enhancement and the sooner this happens. The plateaus are also higher for higher beam energies, reflecting the direct mechanism's expected dependence on beam energy.

Secondly, Fig. 2f shows the cluster motion frequency's strong dependence on beam intensity at 300 kV, clearly illustrating the essential role the irradiation plays through the multiplicative constants. Note that no further Frenkel pairs are created with beam energies at or below 1000 kV.

Finally, Fig. 2g shows the electron energy dependence of $\nu_{\mathrm{MF}}(t \to 0)$, together with the athermal radiation-driven vacancy migration rate under the beam Γ_{vac}. The Γ_{vac} value is proportional to the product of beam flux and the cross section for radiation induced vacancy migration[35],

$$\sigma_{\mathrm{mig}} \approx \int_{E_{\mathrm{mig}}^V}^{E_{\mathrm{K,\,max}}} \frac{E_{\mathrm{K}}}{E_{\mathrm{mig}}^V} \frac{\mathrm{d}\sigma}{\mathrm{d}E_{\mathrm{K}}}\, \mathrm{d}E_{\mathrm{K}},$$

where E_{K} is the kinetic energy transferred from an incident electron to a tungsten atom neighbouring a vacancy, E_{mig}^V is the vacancy migration energy (1.78 eV[36]), and $\mathrm{d}\sigma$ is the differential cross section for the electron-tungsten atom collision calculated using the McKinley-Feshbach formula[37]. The high correlation is clear, further emphasizing the vacancy migration origin of the indirect mechanism.

A natural question is whether this approach has sufficient accuracy to reveal the classical or quantum nature of this rate. The quantity of interest is the logarithm of the motion frequency, which can be written as:

$$\ln \nu_{\mathrm{MF}}(t \to 0) = \ln\left[\Gamma_{\mathrm{th}}^{0}(T) + \Gamma_{\mathrm{d}}\right] \sim \ln \Gamma_{\mathrm{th}}^{0}(T) + \frac{\Gamma_{\mathrm{d}}}{\Gamma_{\mathrm{th}}^{0}(T)}$$

The second term of the right side is easily estimated from the ratio of asymptotic limits $\nu_{\mathrm{MF}}(t \to 0)/\nu_{\mathrm{MF}}(t \to \infty)$. This quantity is in the order of 10^{-1} and 10^{-2} at 1000 keV and 500 keV, respectively, for 289-298 K (Fig. 2d). Also, it is shown to be at most 0.2 at 300 keV even for 31 K (Fig. ED4). This analysis shows that in the measured logarithm of $\nu_{\mathrm{MF}}(t \to 0)$ the effect of the direct de-trapping mechanism is relevant only from the first up to the second decimal place. Hence, the direct and indirect contributions to the motion frequency can be reliably separated.

We provide the statistical procedure in the measurement of $\nu_{\mathrm{MF}}(t)$. One specimen involved 1×10^2 areas for 2000-keV electron irradiation for the SIA cluster production, at maximum. The n value within one area of interest (AOI) centred at a 2000-keV electron irradiated area was $(1 - 2) \times 10^2$ for $t = 0$ s. This n value was the practical upper limit under the lowest TEM magnification enabling the observation of the cluster motion. In the $\nu_{\mathrm{MF}}(t)$ data shown in Figs. 2d-g, Fig. 3, and ED4, each data symbol corresponds to an AOI. The error in the $\nu_{\mathrm{MF}}(t)$ value was evaluated under the assumption that both the distributions of n and n_{m} for a given area independently obey the Poisson distribution. Then, error in a measured $\nu_{\mathrm{MF}}(t)$ value becomes $\nu_{\mathrm{MF}}(t)\sqrt{\frac{1}{n} + \frac{1}{n_{\mathrm{m}}}}$. Series data for temperature dependence of $\nu_{\mathrm{MF}}(t)$ under fixed other conditions (Fig. 3) were taken from the areas belonging to an identical TEM specimen so that the impurity amount over the measured areas was in a very similar level.

Diffusion rates in quantum and classical phonon baths. The archetypal problem of a particle traversing a potential barrier has been treated exhaustively; see Ref. [38] for a thorough review. For a barrier height $\Delta V \gg k_{\mathrm{B}}T$, the classical escape rate is given by the Arrhenius function $\Gamma_{\mathrm{th}}^{\mathrm{cl}} = f_{\mathrm{cl}}\exp(-\Delta V/k_{\mathrm{B}}T)$, where the classical prefactor f_{cl} can be loosely interpreted as an attempt frequency. As $k_{\mathrm{B}}T$ rises towards ΔV the Arrhenius function breaks down, and the rate transitions to a form linear in the temperature[11,23] (manifested as a sharp steepening on an Arrhenius plot). For barriers $\Delta V \sim k_{\mathrm{B}}T$ or less, the particle migrates stochastically, being slowed only by the dissipative coupling between the particle and the underlying phonon bath. This is quantified by the friction parameter γ, and the rate is proportional to $k_{\mathrm{B}}T/\gamma$ [11,23,39]. If $\Delta V \ll k_{\mathrm{B}}T$, the friction can be absorbed into f_{cl}[38,40]. Both standard rate formulae originate from the classical Boltzmann distribution for the phonons. For clusters escaping from traps, the barrier to be overcome is $\Delta V = \Delta V_{\mathrm{P}} + \Delta V_{\mathrm{trap}}$, the sum of the

Peierls barrier and the critical binding energy of the impurity or vacancy respectively. Therefore the diffusion rate is the product of two independent probabilities: the probability related to the free migration of the SIA cluster through the Peierls potential in the absence of a trap, and the escape probability from the trap itself: $\Gamma_{\mathrm{th}}^{\mathrm{cl}}(\mathrm{T}) = \Gamma_{\mathrm{P}}(T) \times \Gamma_{\mathrm{trap}}(T)$. $\Delta V_{\mathrm{trap}} \gg k_{\mathrm{B}}T$, so Γ_{trap} is Arrhenius in the classical limit. Since the Peierls barrier ΔV_{P} for SIA clusters (a.k.a. ½⟨111⟩ loops) is small, i.e. of order $k_{\mathrm{B}}T$, the total classical rate becomes:

$$\Gamma_{\mathrm{th}}^{\mathrm{cl}}(T) = \text{ const. } \times k_{\mathrm{B}}T \times \exp\left(-\frac{\Delta V_{\mathrm{trap}}}{k_{\mathrm{B}}T}\right) \qquad (1)$$

We note that the constant prefactor above can take on a weak temperature dependence in other formulations of the rate; we obtain similar fits in either case and our conclusions are unaffected.

The full quantum-mechanical development is more complicated. Here, the Boltzmann distribution is replaced by either the Bose-Einstein (BE) or Fermi-Dirac distribution, for bosons or fermions respectively. For tungsten or impurity atoms the ground state has integer spin and hence obeys Bose-Einstein statistic. A simple way to recover the BE phonon distribution whilst retaining the form of the classical rate formulae is to renormalize the temperature to mimic the true quantum statistics[15,40,41]. Consider a crystal with periodic boundary conditions represented by *N* atoms in a box. Imposing equality of the classical and quantum energies, the (renormalized, effective) classical temperature and the (true) quantum temperature should be related by the relation:

$$(3N-3)k_{\mathrm{B}}T_c = \int \mathrm{d}\omega\, \hbar\omega \left(\rho_{\mathrm{BE}}(\omega, T_{\mathrm{q}}) + \frac{1}{2}\right) n(\omega)$$

where T_c and T_{q} are the (renormalized, effective) classical and (true) quantum temperatures respectively. $n(\omega)$ is the density of states of the phonon gas, normalized to the number of modes, and $\rho_{BE}(\omega, T)$ is the BE distribution function. Therefore, the effective classical temperature is a function of the true quantum temperature $T_{\mathrm{c}} = f(T_{\mathrm{q}})$.

For temperatures higher than the Debye temperature T_{D}, $\hbar\omega \ll k_B T$, the energy of one oscillator becomes:

$$\hbar\omega \left(\rho_{\mathrm{BE}}(\omega, T_{\mathrm{q}}) + \frac{1}{2}\right) \approx \frac{\hbar\omega}{2} + k_{\mathrm{B}}T_q \left(1 - \frac{\hbar\omega}{2k_{\mathrm{B}}T_{\mathrm{q}}} + K\right) = k_{\mathrm{B}}T_{\mathrm{q}},$$

and the classical and quantum temperatures are very close. When the (true) quantum temperature T_q tends to zero K, the effective classical temperature T_c tends to a finite limit, capturing the zero point energy:

$$(3N-3)k_\mathrm{B}T_\mathrm{c} = \int \mathrm{d}\omega \, \frac{1}{2}\hbar\omega \, n(\omega)$$

The simple form $T_c = \sqrt{\tau_c^2 + T_\mathrm{q}^2}$ satisfies these limits (see Fig. ED5). Therefore, the quantum rates can be estimated by simply renormalizing the temperature in equation (1) yielding:

$$\Gamma_\mathrm{th}^\mathrm{QM}(T) = \text{const.} \times k_\mathrm{B}\sqrt{\tau_\mathrm{c}^2 + T^2} \times \exp\left(-\frac{\Delta V_\mathrm{trap}}{k_\mathrm{B}\sqrt{\tau_\mathrm{c}^2 + T^2}}\right) \qquad (2)$$

We also attempted to fit the data with up to three distinct classical barrier escape mechanisms operating simultaneously. Only the quantum rates explain the observed temperature dependence.

Quantum TST rates. For deep tunneling, we computed the rate by numerically integrating the quantum transition state theory rate expression[40]

$$\Gamma_\mathrm{th}^\mathrm{QTST} = (hZ_0)^{-1}\int W(E)\mathrm{e}^{-E/k_\mathrm{B}T}\mathrm{d}E,$$

where h is the Planck constant and $W(E)$ is the transfer integral at energy E for the sech-squared impurity interaction potential predicted by the Frenkel Kontorova model, (see Supplementary Discussion 1). The data can be fitted with a barrier height of 55 meV, but requires an unrealistically low effective cluster mass of $m_\mathrm{W}/200$ (m_W is the mass of one tungsten atom). The remaining parameters (potential width and curvature) are fixed by the Arrhenius limit, which applies to the highest temperature points in the dataset.

References

30 Amino, T., Arakawa, K. & Mori, H. Activation energy for long-range migration of self-interstitial atoms in tungsten obtained by direct measurement of radiation-induced point-defect clusters. *Philosophical Magazine Letters* **91**, 86-96, doi:10.1080/09500839.2010.533133 (2011).

31 Maury, F., Biget, M., Vajda, P., Lucasson, A. & Lucasson, P. Frenkel pair creation and stage I recovery in W crystals irradiated near threshold. *Radiation Effects* **38**, 53-65, doi:10.1080/00337577808233209 (1978).

32 Arakawa, K., Amino, T. & Mori, H. Direct observation of the coalescence process between nanoscale dislocation loops with different Burgers vectors. *Acta Mater* **59**, 141-145, doi:10.1016/j.actamat.2010.09.018 (2011).
33 Hirsch, P. B., Howie, A., Nicholson, R. B., Pashley, D. W. & Whelan, M. J. *Electron Microscopy of Thin Crystals*. (Butterworths, London, 1965).
34 Jenkins, M. L. & Kirk, M. A. *Characterization of Radiation Damage by Transmission Electron Microscopy*. (Institute of Physics, Bristol and Philadelphia, 2001).
35 Kiritani, M. Electron Radiation Induced Diffusion of Point Defects in Metals. *Journal of the Physical Society of Japan* **40**, 1035-1042, doi:10.1143/JPSJ.40.1035 (1976).
36 Nguyen-Manh, D., Horsfield, A. P. & Dudarev, S. L. Self-interstitial atom defects in bcc transition metals: Group-specific trends. *Physical Review B* **73**, 020101 (R) (2006).
37 Oen, O. S. Cross sections for atomic displacements in solids by fast electrons. (1965).
38 Hänggi, P., Talkner, P. & Borkovec, M. Reaction-rate theory: fifty years after Kramers. *Reviews of Modern Physics* **62**, 251-341 (1990).
39 Dudarev, S. L. Coherent motion of interstitial defects in a crystalline material. *Philos Mag* **83**, 3577-3597, doi:10.1080/14786430310001599388 (2003).
40 Benderskii, V., Makarov, D. & Wight, C. *Chemical Dynamics at Low Temperature*. (Wiley-Interscience, 1994).
41 Wang, C. Z., Chan, C. T. & Ho, K. M. Tight-binding molecular-dynamics study of phonon anharmonic effects in silicon and diamond. *Physical Review B* **42**, 11276-11283 (1990).

Figures

a

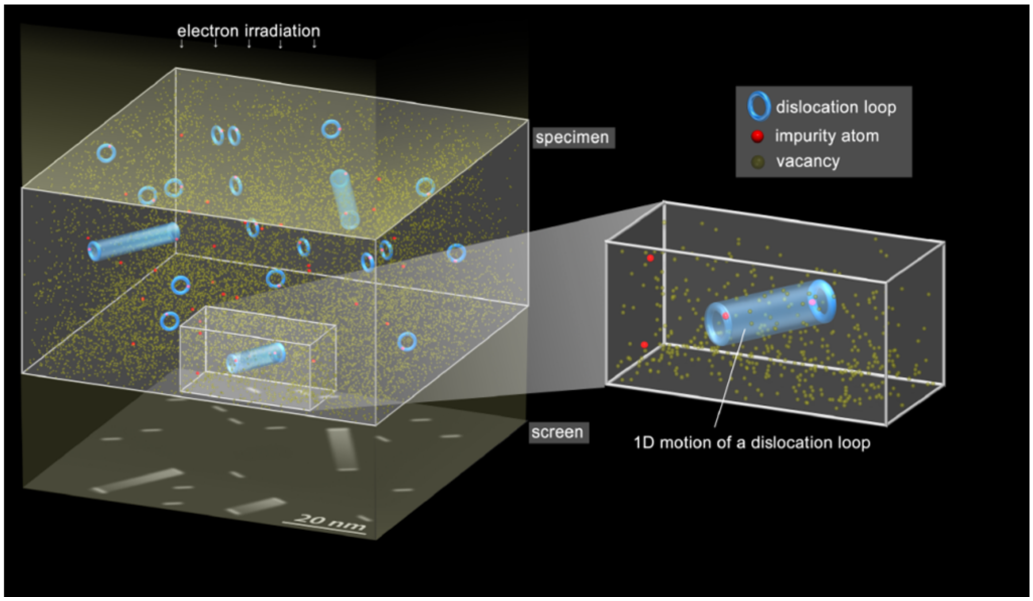

b

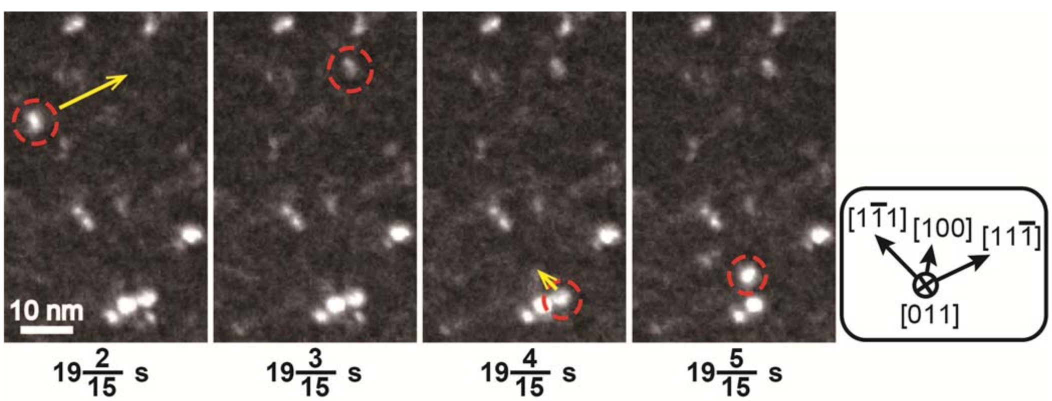

Figure 1 | 1D SIA cluster motion. a: Experimental setup. In a high-purity tungsten specimen, SIA clusters in the form of nanoscale ½⟨111⟩dislocation loops are trapped by impurity atoms at their boundary. **b**: High-energy electron irradiation enables clusters to escape, and subsequently undergo fast 1D glide diffusion before being trapped by other impurity atoms. This 1D motion was monitored simultaneously (acceleration voltage: 1000 kV; beam intensity: 2×10^{25} $m^{-2}s^{-1}$; temperature: 260 K, see Supplementary Video 1). Circled clusters move in the directions indicated by arrows, parallel to the $\langle 111 \rangle$-type cluster Burgers vectors. The clusters hop distances of several nm to a few tens of nm within a single 1/15 s movie frame.

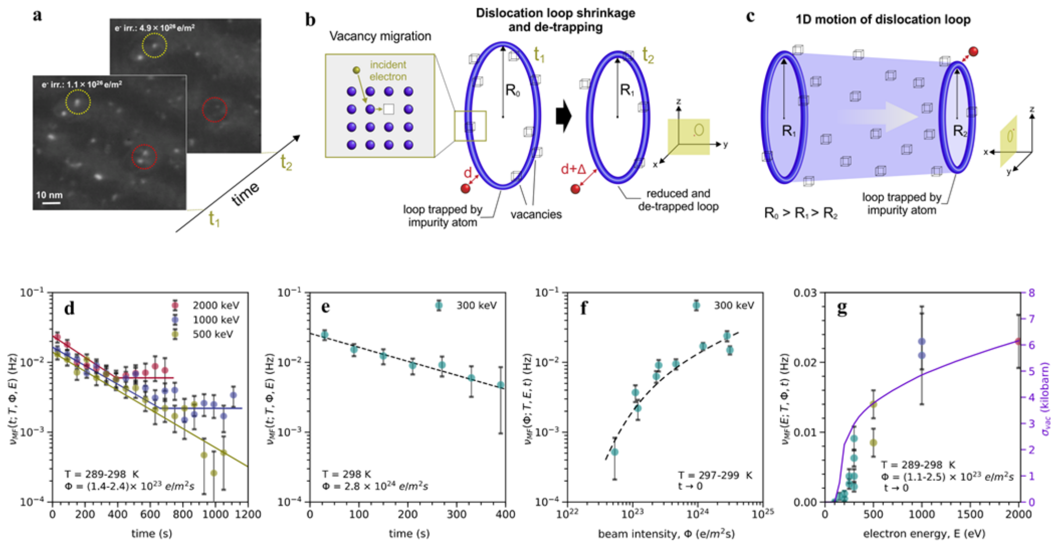

Figure 2 | Characterization of the motion frequency of SIA cluster de-trapping. **a:** SIA cluster (dislocation loop) shrinking under the beam (acceleration voltage: 300 kV; beam intensity: 3.1×10^{24} $m^{-2}s^{-1}$; temperature: 299 K). Vacancies in tungsten are thermally immobile at 299 K, and so the only way the SIA clusters can shrink is via the absorption of radiation-mobilized vacancies. **b:** The clusters escape by increasing the distance between their perimeter and the impurity, from d to $d + \Delta$, as they shrink from radius R_0at time $t_1 \rightarrow R_1 < R_0$ at time t_2. This reduces the binding energy (see Supplementary Discussion 1) **c:** Stop-and-go motion of the loop in the clouds of vacancies and impurities. Once the loop has escaped from the impurity, it migrates until is trapped by another impurity. During this macro-jump, over many Peierls barriers, the loop sweeps through the surrounding vacancy clouds, decreasing its effective radius to $R_2 < R_1$. **d, e:** Motion frequency decaying exponentially with time under irradiation which corresponds to indirect mechanism (see Methods). Plateaus are reached when the supply of vacancies local to the clusters is exhausted by annihilation, and the direct mechanism takes over (see Methods). **f:** Motion frequency increasing with beam intensity (time: 0 – 60 s). **g:** Motion frequency vs. beam energy and cross section for radiation-induced vacancy migration (time: 0 – 60 s) (see Methods).

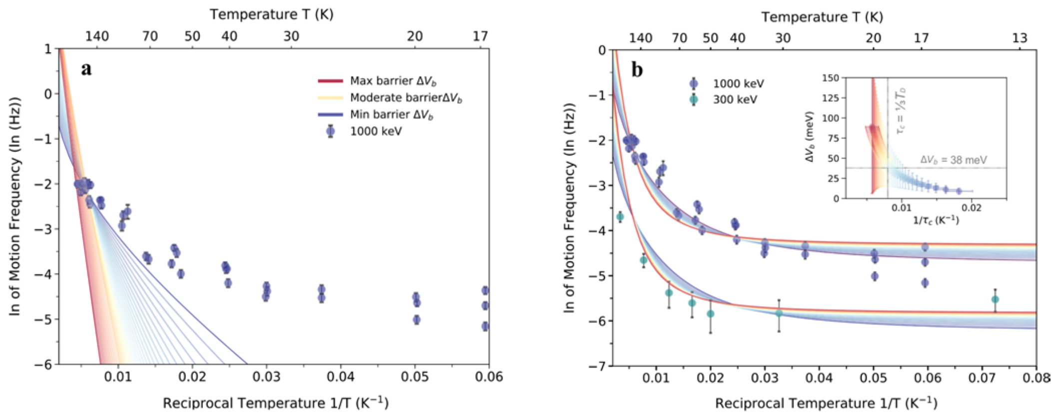

Figure 3 | **Motion frequency of SIA cluster de-trapping vs. temperature.** Data points show measured motion frequency vs. temperature (data taken in first 60 s of irradiation. Blue points: beam energy 1000 keV, beam intensity 2×10^{25} m^{-2}s^{-1}; green points: beam energy 300 keV, beam intensity $(2-4) \times 10^{24}$ m^{-2}s^{-1}). Some error bars are too small to be visible. **a**: All possible classical fits of one single dataset, at beam energy of 1000 keV, for activation barriers between 10 meV (blue) and 90 meV (red). Thin lines between are intermediate values. No classical fit can capture the temperature dependence. **b**: As panel a but using quantum mechanical rate function. Both 1000 and 300 keV datasets were fitted simultaneously, with a single parameter to account for the ratio of the two (we obtained a value of 4.52 for the ratio, consistent with Fig. 2g, see Methods). Inset: fitted correlation between activation barrier and critical temperature τ_c (see text and Methods), with corresponding error bars. The value of the effective activation barrier at $\tau_c = \frac{1}{3}T_D$ (T_D: Debye temperature) is 38 meV.

Extended Display Items

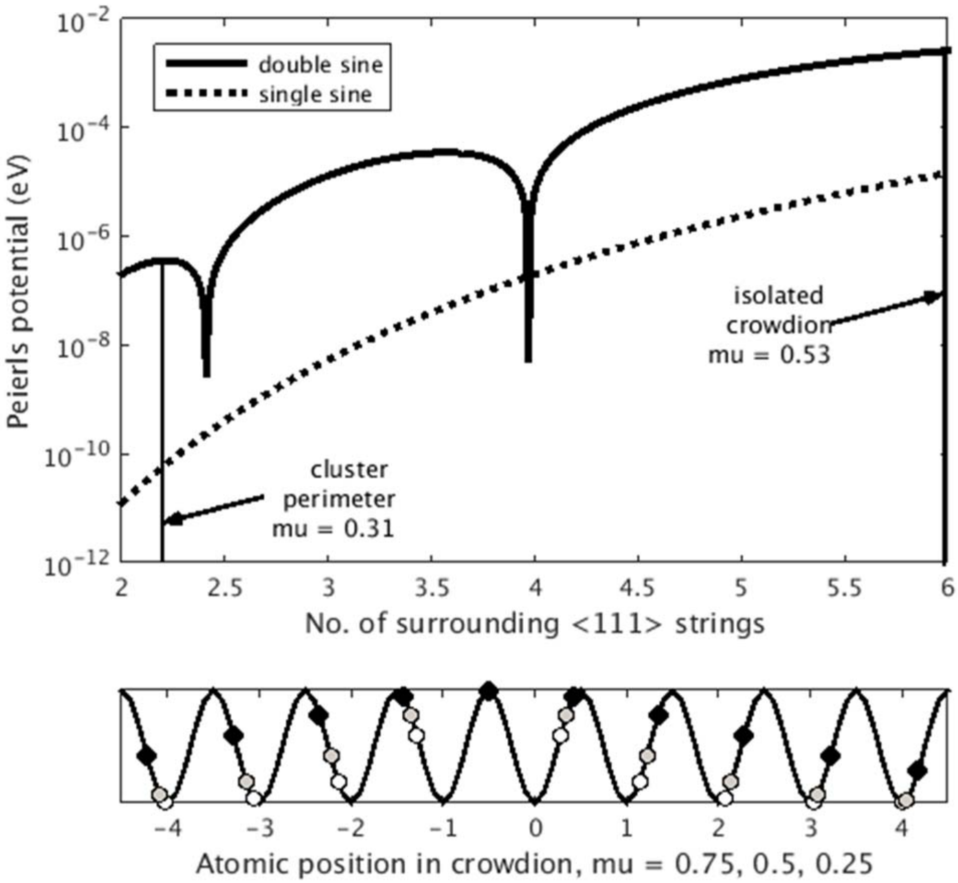

Figure ED1 | Top: suppression of Peierls potential as delocalization increases (and μ decreases). Both the standard single-sine and more accurate double-sine Frenkel-Kontorova models predict a negligibly small barrier for cluster diffusion after escape from the traps. Bottom: atomic positions showing increased delocalization as μ decreases from 0.75 (open circles) through 0.5 (grey circles) to 0.25 (solid circles).

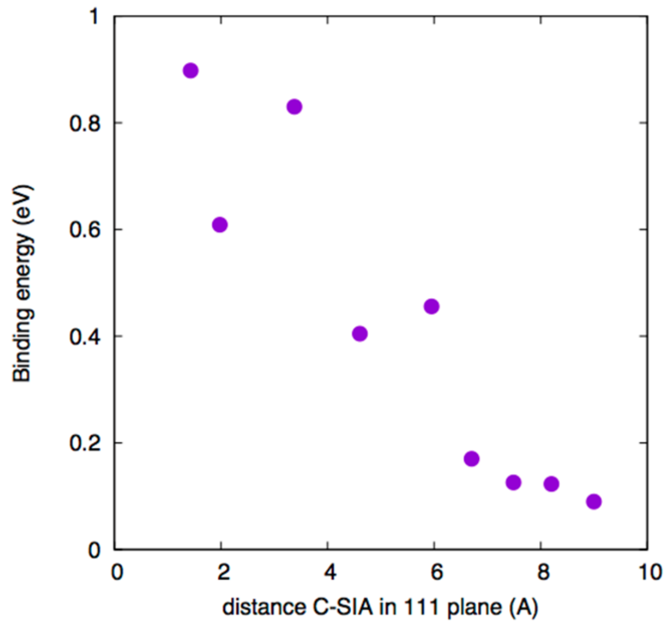

Figure ED2a | DFT calculation of the SIA-carbon binding energy vs. separation in plane transverse to the crowdion axis.

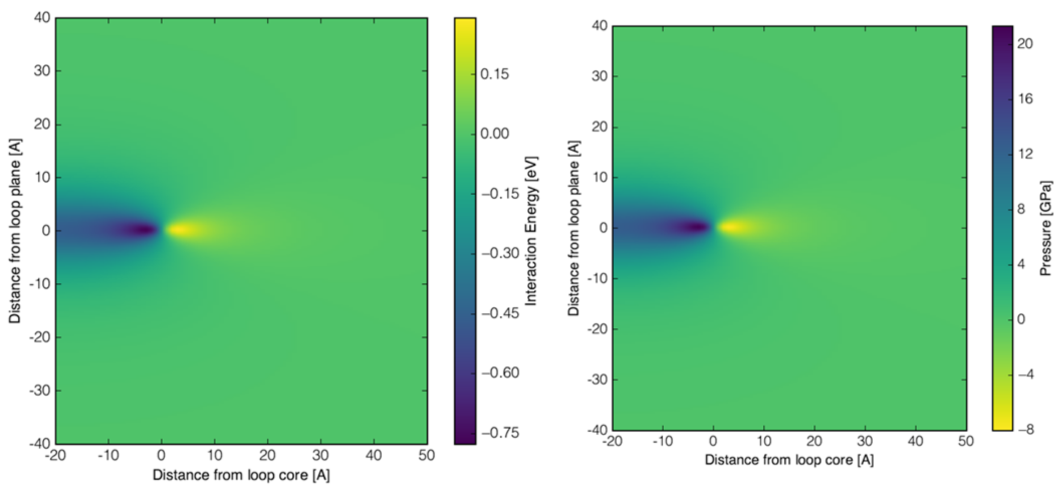

Figure ED2b | Elastic calculation of the SIA cluster-dilatation centre binding energy (left) and cluster pressure field (right).

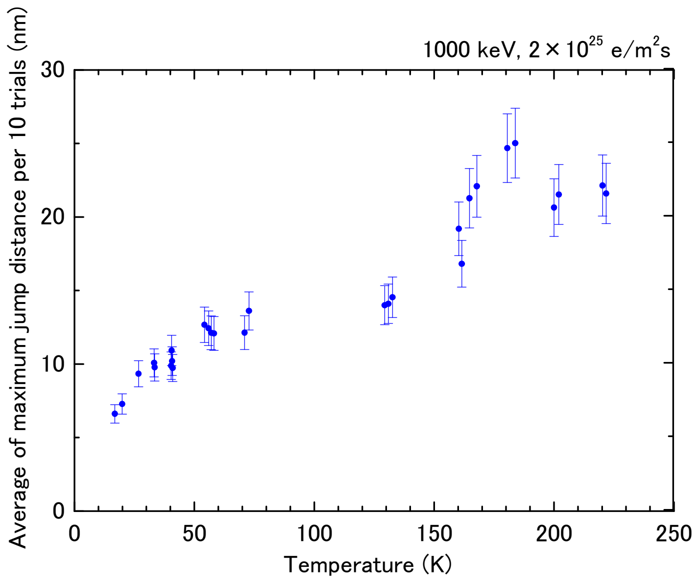

Figure ED3 | Average maximum hop distance per 10 hops vs temperature. A range of binding energies exist, corresponding to different cluster-impurity separations. This means more impurities are effective traps at lower temperatures, leading to a reduced hop distance.

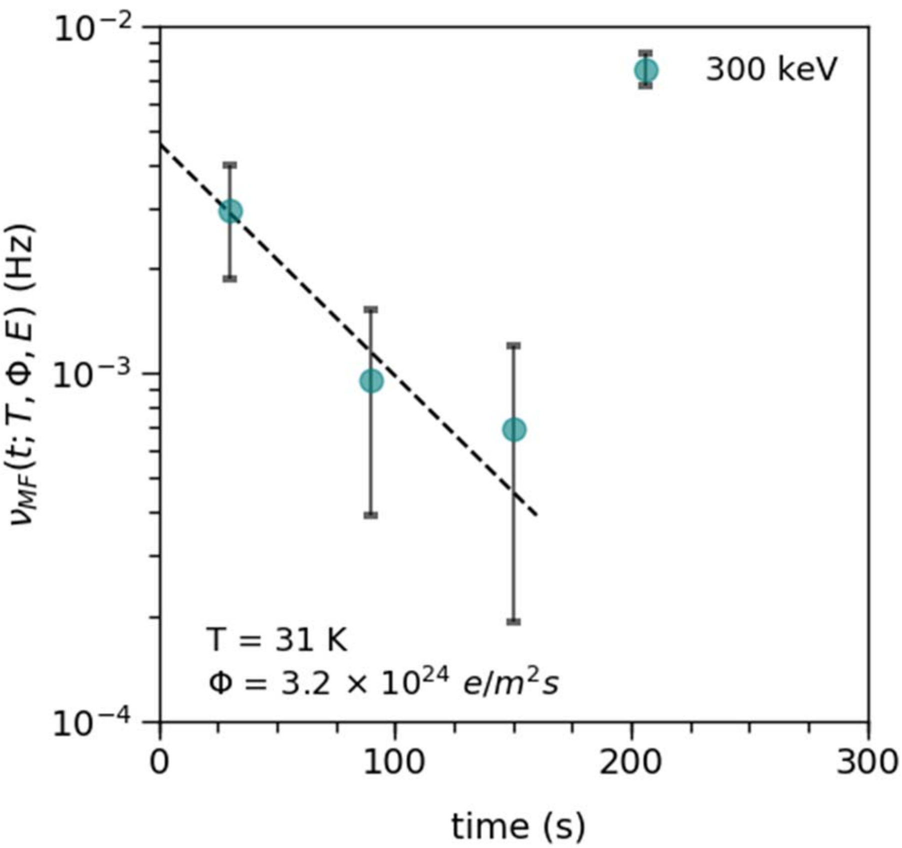

Figure ED4 | Motion frequency vs irradiation time at 31 K, with beam energy 300 keV. The decrease in motion frequency, attributed to the depletion of vacancies near the clusters, is still clear, and demonstrates that the direct mechanism (which would induce a motion frequency constant in time) is not wholly responsible for the cluster motion. Indeed, at short times the motion is dominated by the indirect mechanism, by at least a factor of 5.

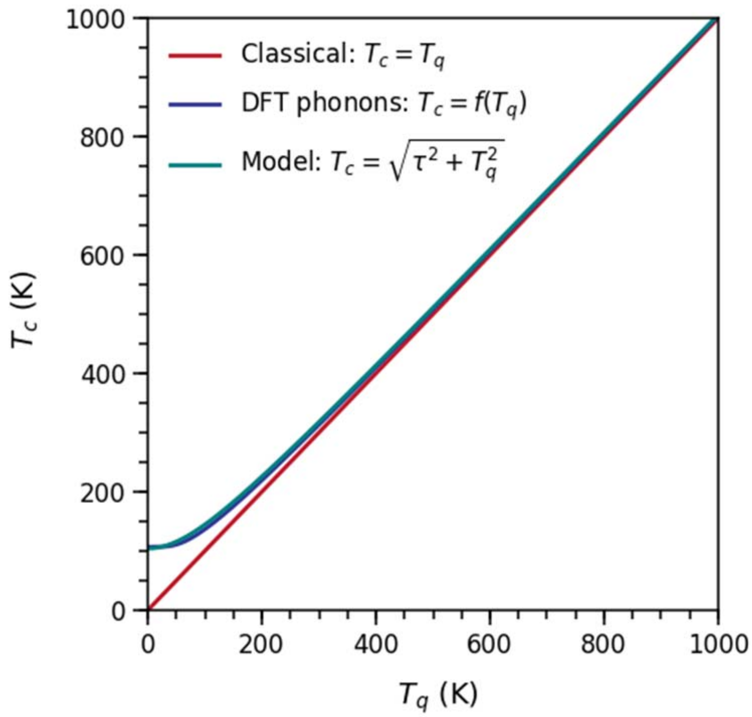

Figure ED5 | The correspondence between the effective classical temperature T_c (our model) and the quantum (true) temperature T_q of perfect bulk bcc W. The classical, DFT phonons and our model are shown in red, dark blue and light blue respectively.